

# Kinematic Analysis and Control of an Omnidirectional Mobile Robot in Rough Terrain

Martin Udengaard and Karl Iagnemma

*Massachusetts Institute of Technology  
77 Massachusetts Ave, Cambridge, MA 02139  
mru, kdi@mit.edu*

**Abstract**—An omnidirectional mobile robot is able, kinematically, to move in any direction regardless of current pose. To date, nearly all designs and analyses of omnidirectional robots have considered the case of motion on flat, smooth terrain. This paper presents a kinematic analysis and control method for an omnidirectional mobile robot driven by active split offset casters operating on rough, uneven terrain. Robot average isotropy is analyzed as a function of wheel module geometry on both flat and rough terrain. A simple kinematic control scheme that considers the effects of terrain unevenness is presented. The performance of the algorithm in rough terrain is studied in simulation. It is shown that with knowledge of terrain conditions, near-omnidirectional mobility is achievable in rough terrain.

*Index Terms*—Omnidirectional vehicle, rough terrain, isotropy, mobile robots

## I. INTRODUCTION

Mobile robots are finding increasing use in military [1], disaster recovery [2], and exploration applications [3]. These applications frequently require operation in rough, unstructured terrain. Currently, most mobile robots designed for these applications are tracked or Ackermann-steered wheeled vehicles. Methods for controlling these types of robots in both smooth and rough terrain have been well studied [4-7]. While these robots types can perform well in many scenarios, navigation in cluttered, rocky, or obstacle-dense urban environments can be difficult or impossible. This is partly due to the fact that traditional tracked and wheeled robots must reorient to perform some maneuvers, such as lateral displacement. Omnidirectional mobile robots could potentially navigate faster and more reliably through cluttered urban environments and over rough terrain, due to their ability to track near-arbitrary motion profiles.

An omnidirectional mobile robot is able, kinematically, to move in any direction regardless of current pose. Previous researchers have proposed and developed omnidirectional mobile robots employing a wide variety of wheel types including roller [8,9], Mecanum [10,11], and spherical wheels [12,13].

Roller wheel designs employ small rollers along the outer

edge of a “primary” wheel to allow traction in the wheel’s longitudinal direction and free rolling in the lateral direction. Omnidirectional motion is obtained by orienting several of these wheels in different directions. These wheels are inexpensive, easy to control, and operate well in flat, indoor environments. Mecanum wheels are similar to roller wheels in that they employ rollers along the outer edge of a wheel; however the rollers are aligned at an angle to produce angular contact forces with the ground. Robots equipped with four Mecanum wheels can produce omnidirectional motion. Again, these wheel types have proved to be simple to control and effective on flat, clean terrain. In outdoor environments, debris can clog the rollers and alter the friction characteristics of the wheels [14]. Also, the (relatively) small rollers on the edge of each primary wheel can be subjected to significant loads, which can lead to high ground pressure and large sinkage in deformable outdoor terrain.

Spherical wheel designs employ frictional drive rollers to allow rolling in any direction. Since the drive rollers rely on friction to transmit energy to the wheel, debris could potentially foul the transmission mechanism in rough, outdoor environments.

Near-omnidirectional motion has been achieved using steerable wheels [15]. These designs have a wheel that can be steered in any direction by an orthogonal steering actuator. These wheels can employ standard tires, and have proven effective in outdoor environments. However they are not truly omnidirectional (i.e. the resulting vehicle kinematics are subject to nonholonomic constraints), and must sometimes undergo wheel slip and/or scrubbing to change direction. Note that similar designs based on offset caster wheels do allow omnidirectional motion with standard tires [16]. Analysis of this design has been studied extensively for operation on flat ground.

An omnidirectional mobile robot driven by active split offset casters (ASOCs) was initially proposed in [17] for use in structured, indoor environments. ASOC drives employ conventional wheel designs that do not rely on frictional contact, and are thus potentially suitable for use in dirty, outdoor environments. They also can be designed with little constraint on wheel diameter and width, and thus can potentially tolerate large loads with low ground pressure. Finally, ASOC modules can be integrated with suspension systems that allow for traversal of uneven terrain [18].

Therefore ASOC-driven omnidirectional mobile robots hold promise for use in rough, unstructured environments.

In this paper a kinematic analysis of an ASOC-driven omnidirectional mobile robot is presented, along with an analysis of the robot's isotropy characteristics in rough terrain. These analyses can be used as design guidelines for development of an omnidirectional mobile robot that can operate in unstructured environments. A simple kinematic controller that considers the effects of terrain unevenness via an estimate of the wheel-terrain contact angles is also presented. It is shown in simulation that under the proposed control method, near-omnidirectional tracking performance is possible even in rough, uneven terrain.

## II. ACTIVE SPLIT OFFSET CASTER DESCRIPTION

ASOC drive modules possess the ability to achieve omnidirectional motion via a driven wheel pair. Figure 1 shows the ASOC module considered in this study. The assembly consists of a split wheel pair, a connecting axle, and an offset link connecting the wheel pair to the mobile robot body. Each wheel is independently driven about the axis  $\theta$ . The axle connecting the wheel pair can pivot about the axis  $\beta$ . This joint can be passive or active, and allows the wheel pair to adapt to terrain unevenness, therefore ensuring continuous terrain contact for each wheel even during travel on rough terrain. The wheel pair/axle assembly rotates passively about axis  $\alpha$ . This axis connects the ASOC module to a robot body or a passive or active suspension element.  $L_{offset}$  is the distance between the axis  $\alpha$  and the axis  $\theta$ .  $L_{split}$  is the distance between the wheels.

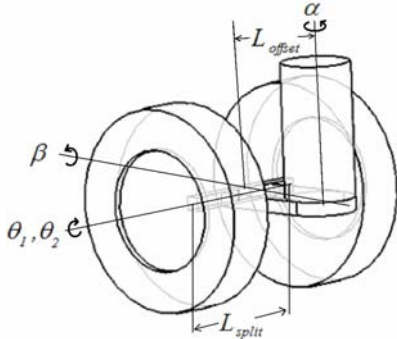


Figure 1. Active split offset caster wheel assembly.

By independently controlling each wheel's velocity, an ASOC module can produce arbitrary (planar) translational velocities at a point along its  $\alpha$  axis [17]. Two or more ASOCs attached to a rigid robot body can thus produce arbitrary translational and rotational robot velocities. Therefore, an ASOC-driven omnidirectional robot must minimally employ two ASOC modules, and can employ more to meet other design requirements related to thrust, ground pressure, tip-over stability, etc. Note that passive or active casters can also be used to augment ASOC modules to meet these requirements.

## III. KINEMATIC MODELING

Figure 2 shows an illustration of an omnidirectional mobile robot driven by four ASOC modules. This is the configuration that will be considered in this work; however the analysis is general and applies to robots with  $N$  ASOCs.

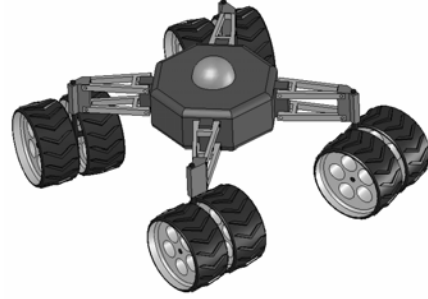


Figure 2. Illustration of an ASOC-driven omnidirectional mobile robot. This robot has four ASOC modules spaced at  $90^\circ$  intervals.

The coordinate frames were defined using Denavit-Hartenberg (D-H) notation and shown in Table I. Coordinate frame assignments are shown in Figure 3.

TABLE I  
JOINT REPRESENTATION IN D-H NOTATION

Joint number	$d_i$	$\zeta_i$	$a_i$	$\xi_i$
$1_n$	0	$2\pi(n-1)/N$	$r$	0
$2_n$	$h$	$-(\alpha + \pi/2)$	0	$\pi/2$
$3_n$	$L_{offset}$	$-\beta$	0	0
$4_{n,m}$	0	0	$\pm L_{split}/2$	0

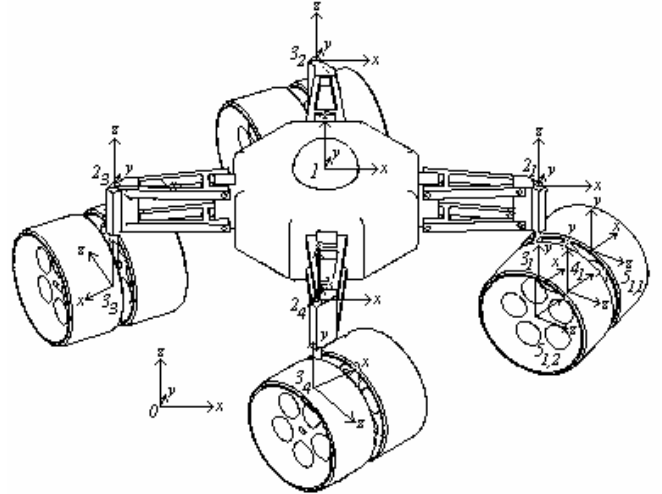


Figure 3. Coordinate frame assignments for an ASOC-driven omnidirectional mobile robot. Note that some wheel and axle frames are hidden for clarity.

In the notation above,  $d_i$  is the distance between frame  $i$  and frame  $i+1$  along the  $z_{i+1}$  axis,  $\zeta_i$  is the angle between  $x_i$  and  $x_{i+1}$  about  $z_{i+1}$ ,  $a_i$  is the distance from  $z_i$  to  $z_{i+1}$  along  $x_{i+1}$ ,  $\xi_i$  is the twist angle between  $z_i$  and  $z_{i+1}$  about  $x_{i+1}$ ,  $n$  is the ASOC number,  $m$  is the wheel number,  $r$  is the body radius, and  $h$  is the vertical distance from the ASOC base to the

vehicle body.

Here a three-dimensional model is considered. A body-fixed frame (“1”) is allowed 6 DOF with respect to an inertial frame (“0”). The interface of each ASOC module link and the robot body/suspension frame (“2<sub>*n*</sub>” where *n* refers to the ASOC number and *N* is the total number of ASOCs) is defined on the body a distance *r* from the center of the body. A frame (“3<sub>*n*</sub>”) at the bottom of each ASOC module link is a distance *h* below the previous frame and can rotate about axis  $\alpha$ . The next frame (“4<sub>*n*</sub>”) is defined on the axle at the midpoint between the wheels, and can rotate about  $\beta$ . For convenience, a frame is also defined at the center of each wheel (“5<sub>*n,m*</sub>”) where *n* refers to the ASOC number and *m* refers to the wheel number). These redundant frames are fixed with respect to the axle frame. There is no specified wheel-ground contact frame, as each wheel may have no contact or several moving contact points.

Coordinate transformation matrices are defined as follows:

$$T_1^{2_n} = \begin{bmatrix} \cos[2\pi(n-1)/N] & -\sin[2\pi(n-1)/N] & 0 & r \\ \sin[2\pi(n-1)/N] & \cos[2\pi(n-1)/N] & 0 & 0 \\ 0 & 0 & 1 & 0 \\ 0 & 0 & 0 & 1 \end{bmatrix} \quad (1)$$

$$T_2^{3_n} = \begin{bmatrix} \cos[-(\alpha_n + \pi/2)] & 0 & \sin[-(\alpha_n + \pi/2)] & 0 \\ \sin[-(\alpha_n + \pi/2)] & 0 & -\cos[-(\alpha_n + \pi/2)] & 0 \\ 0 & 1 & 0 & h \\ 0 & 0 & 0 & 1 \end{bmatrix} \quad (2)$$

$$T_3^{4_n} = \begin{bmatrix} \cos(-\beta_n) & -\sin(-\beta_n) & 0 & 0 \\ \sin(-\beta_n) & \cos(-\beta_n) & 0 & 0 \\ 0 & 0 & 1 & L_{offset} \\ 0 & 0 & 0 & 1 \end{bmatrix} \quad (3)$$

$$T_4^{5_{n,m}} = \begin{bmatrix} 1 & 0 & 0 & (-1)^m \frac{L_{split}}{2} \\ 0 & 1 & 0 & 0 \\ 0 & 0 & 1 & 0 \\ 0 & 0 & 0 & 1 \end{bmatrix} \quad (4)$$

where  $T_p^q$  is the matrix transforming motion from frame *p* into frame *q*. Thus the transformation from the body center frame to the wheel<sub>*n,m*</sub> frame is

$$T_1^{5_{n,m}} = T_1^{2_n} T_2^{3_n} T_3^{4_n} T_4^{5_{n,m}} \quad (5)$$

Using these relations, the wheel velocities required to generate a desired body center velocity can be determined.

#### IV. ISOTROPY ANALYSIS

Kinematic isotropy is defined as the condition where a

robot possesses a constant input velocity/output velocity ratio for all possible output velocity directions [16]. An isotropy metric is a measure of how near a robot is to the isotropy condition, and increases from 0.0 for a singular configuration (i.e. purely anisotropic, or non-omnidirectional) to 1.0 for kinematic isotropy. Ideally, an omnidirectional robot should possess a metric value of 1.0 for all joint space configurations, and thus not have a preferred direction of travel. This simplifies path planning and navigation by eliminating the effect of robot orientation on movement capability. The output directions considered in this study are two planar translations in the x-y plane in the robot body frame, and rotation about the robot body frame z axis.

The isotropy metric for a given robot configuration can be computed as the ratio of the smallest to largest eigenvalues of the Jacobian matrix [16]. The isotropy metric can be averaged over the entire configuration space (in this case, the rotation angles between each ASOC and the body,  $\alpha$ ) to yield an average measure of performance that could be used to compare candidate omnidirectional mobile robot designs.

To analyze the effects of ASOC module kinematic parameters on isotropy,  $L_{offset}$  and  $L_{split}$  were varied over a range of values that represent a practical omnidirectional robot design space. Note that in Figure 3,  $L_{offset}$  and  $L_{split}$  are normalized by the robot body length, defined as the length of the longest side of the robot body.

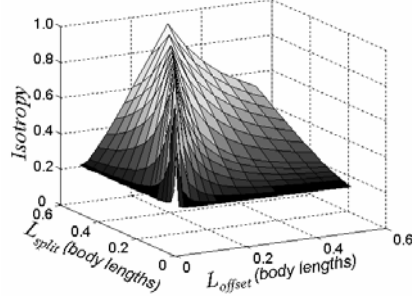


Figure 3. Average isotropy for a four ASOC omnidirectional robot.

An iso-height exists at an isotropy value of 1.0. This iso-height occurs at  $L_{split} / L_{offset} = 2.0$ . The sensitivity of isotropy to perturbations in  $L_{split}$  and  $L_{offset}$  is relatively high; a 10% change in  $L_{split}$  or  $L_{offset}$  decreases the isotropy metric value by up to 45% for small ASOC module sizes.

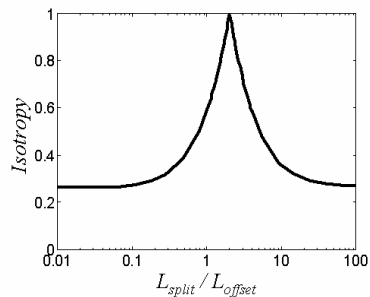


Figure 4. Average isotropy for omnidirectional robot driven by four ASOC modules as a function of  $L_{split} / L_{offset}$ .

Figure 4 is a plot of isotropy values over a range of  $L_{split}$  and  $L_{offset}$  values. From this figure it can be seen that there exists a single isotropy value for each  $L_{split} / L_{offset}$  ratio, indicating that isotropy is not an independent function of both  $L_{split}$  and  $L_{offset}$ . This is a useful insight for omnidirectional robot design. This also explains the sensitivity of isotropy to changes in  $L_{split}$  and  $L_{offset}$  for small ASOC modules sizes, since a unit change in  $L_{split}$  or  $L_{offset}$  results in a relatively large change in  $L_{split} / L_{offset}$  for small parameter values.

Isotropy of an omnidirectional robot can also be affected by terrain roughness. Variation in terrain inclination among ASOC module wheels, or among ASOC module wheel pairs, causes a change in the effective value of  $L_{split}$  with respect to the body frame, which yields a change in  $L_{split} / L_{offset}$  and thus a change in isotropy (see Figure 5). As mentioned in Section II, axis  $\beta$  allows ASOC wheels to maintain ground contact during travel on uneven terrain.

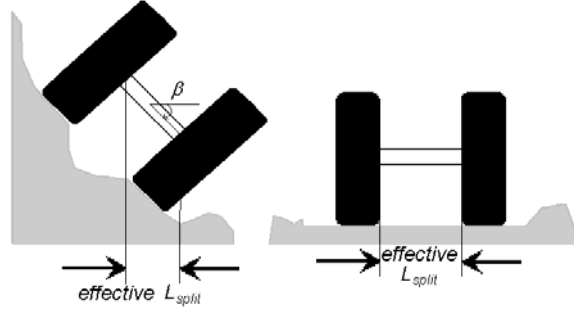


Figure 5. ASOC module on flat and rough terrain. Rough terrain causes the wheel pair to pivot about the  $\beta$  axis, decreasing the effective  $L_{split}$ .

In theory,  $L_{split}$  could be modified as a function of terrain inclination via an active, extensible axle to cause the effective  $L_{split} / L_{offset}$  ratio to always be near 2.0, thus yielding good isotropy characteristics on rough terrain. In practice, however, such a design would be cumbersome and impractical. Thus it is useful to examine the effects of terrain inclination on robot isotropy.

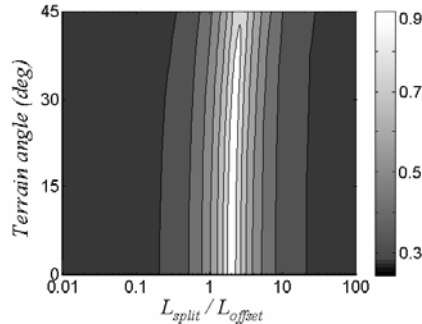


Figure 6. Average isotropy as a function of  $L_{split} / L_{offset}$  and terrain angle.

In Figure 6, a contour plot is presented of the average isotropy over a range of static robot configurations and terrain angles. It can be seen that the  $L_{split} / L_{offset}$  ratio with the largest isotropy value increases with the maximum terrain angle. Larger angles decrease the effective ratio and thus the “true” ratio must therefore increase. Maximum average isotropy also decreases slightly with increasing

terrain angle. Table II summarizes these findings.

Terrain angle	Max isotropy	Optimum
		$L_{split} / L_{offset}$ ratio
0° (flat)	1.000	2.00
0-15°	0.987	2.05
0-30°	0.950	2.27
0-45°	0.895	2.70

#### V. KINEMATIC CONTROL OF AN ASOC-DRIVEN OMNIDIRECTIONAL MOBILE ROBOT ON ROUGH TERRAIN

A simple kinematic control scheme has been developed based on the preceding kinematic analysis. Given a desired body translational and rotational velocity defined in an inertial frame, the velocity for each ASOC wheel can be determined despite the effects of terrain unevenness.

First, the velocity of the link between the ASOC module and robot body is computed by:

$$\dot{\mathbf{x}}_{link} = \dot{\mathbf{x}}_{body} + \dot{\phi} \mathbf{r} \begin{bmatrix} \cos(\zeta_i) \\ \sin(\zeta_i) \end{bmatrix} \quad (6)$$

where  $\dot{\mathbf{x}}_{link}$  and  $\dot{\mathbf{x}}_{body}$  are the planar velocity vectors of the link and body, respectively,  $\dot{\phi}$  is the yaw rate of the body, and  $r$  and  $\zeta_i$  locate the link  $i$  in the body frame. The wheel velocities that yield the desired ASOC link velocity are found as [17]:

$$\dot{\mathbf{x}}_{link} = \begin{bmatrix} \frac{1}{2} \cos(\alpha_n) - \frac{L_{offset}}{L_{split}} \sin(\alpha_n) & \frac{1}{2} \cos(\alpha_n) + \frac{L_{offset}}{L_{split}} \sin(\alpha_n) \\ \frac{1}{2} \sin(\alpha_n) + \frac{L_{offset}}{L_{split}} \cos(\alpha_n) & \frac{1}{2} \sin(\alpha_n) - \frac{L_{offset}}{L_{split}} \cos(\alpha_n) \end{bmatrix} \begin{bmatrix} V_{n,1} \\ V_{n,2} \end{bmatrix} \quad (7)$$

and hence:

$$\begin{bmatrix} V_{n,1} \\ V_{n,2} \end{bmatrix} = \begin{bmatrix} \frac{1}{2} \cos(\alpha_n) - \frac{L_{offset}}{L_{split}} \sin(\alpha_n) & \frac{1}{2} \cos(\alpha_n) + \frac{L_{offset}}{L_{split}} \sin(\alpha_n) \\ \frac{1}{2} \sin(\alpha_n) + \frac{L_{offset}}{L_{split}} \cos(\alpha_n) & \frac{1}{2} \sin(\alpha_n) - \frac{L_{offset}}{L_{split}} \cos(\alpha_n) \end{bmatrix}^{-1} \dot{\mathbf{x}}_{link} \quad (8)$$

where  $V_{n,m}$  is the forward linear velocity of a wheel $_{n,m}$  in the wheel frame (“ $S_{n,m}$ ”), and is computed as  $V_{n,m} = R\omega_{n,m}$  where  $R$  is the wheel radius and  $\omega_{n,m}$  is the wheel angular speed. Angular velocity is controllable via simple PD or other schemes. This motion also tends to rotate the ASOCs in the direction of travel with the  $\alpha$  axis in front.

Terrain roughness causes ASOC modules to tilt (i.e. rotate about  $\beta$ ) and the wheel velocities to have components not in the body’s  $x$ - $y$  plane. Module tilt is compensated via computation of an effective  $L_{split}$ , (see Figure 5). Inclination

effects are compensated via projection of the wheel velocity onto the body's  $x$ - $y$  plane. Applying these modifications to (8) yields:

$$\begin{bmatrix} V_{n,1} \cos \gamma_{n,1} \\ V_{n,2} \cos \gamma_{n,2} \end{bmatrix} = \begin{bmatrix} \frac{1}{2} \cos(\alpha_i) - \frac{L_{offset}}{L_{split}} \frac{\sin(\alpha_i)}{\cos(\beta_i)} & \frac{1}{2} \cos(\alpha_i) + \frac{L_{offset}}{L_{split}} \frac{\sin(\alpha_i)}{\cos(\beta_i)} \\ \frac{1}{2} \sin(\alpha_i) + \frac{L_{offset}}{L_{split}} \frac{\cos(\alpha_i)}{\cos(\beta_i)} & \frac{1}{2} \sin(\alpha_i) - \frac{L_{offset}}{L_{split}} \frac{\cos(\alpha_i)}{\cos(\beta_i)} \end{bmatrix}^{-1} \dot{\mathbf{x}}_{link} \quad (9)$$

where  $\gamma_{n,m}$  is the angle between the forward motion of wheel $_{n,m}$  and the  $x$ - $y$  plane of the body (see Figure 7).

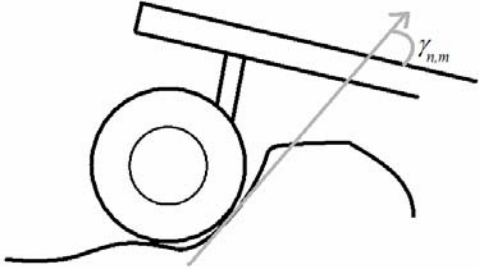


Figure 7. Wheel inclination angle,  $\gamma_{n,m}$ .

Figure 8 shows a block diagram of a scheme for rough terrain omnidirectional mobile robot control. The input is a desired velocity profile defined in the inertial frame. It is assumed that the robot's full state can be estimated. The desired velocity profile is converted to a desired body frame velocity based on the robot's current position and orientation. ASOC module link velocities are then computed via (6). Desired wheel velocities can then be calculated using (9), here assuming knowledge or estimates of local terrain inclination. Terrain inclination can be estimated via axle-mounted force sensors (to measure wheel-terrain interaction normal force direction) or via kinematic estimators [19]. PD controllers command each to track the desired wheel velocities. Actual wheel velocity can be determined via odometry; however more sophisticated methods are required to estimate wheel slip.

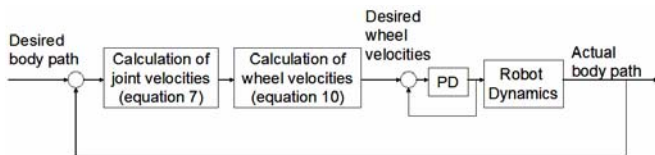


Figure 8. Control scheme of an omnidirectional mobile robot.

## VI. SIMULATION RESULTS

A dynamic model of an ASOC-driven mobile robot was developed to study the performance on the control method described above. The kinematic controller described in Section IV was implemented to allow the robot to track a desired velocity profile over flat and rough terrain. Independent PD control loops allowed each wheel to track its desired velocity.

The robot parameters for the simulation were as follows: body length=1 m, total mass=22 kg, wheel radius=0.10 m,  $L_{split}$ =0.20 m,  $L_{offset}$ =0.10 m. The control gains for each wheel were  $K_p=7.3$ ,  $K_d=0.02$ . Wheel-terrain interaction forces were determined via a simple coulomb friction model. Terrain elevation was modeled as a zero-mean triangularized mesh with elevation points possessing a standard deviation of  $\sigma$ . In initial simulations it was assumed that the robot possessed perfect knowledge of terrain inclination. Wheel-terrain contact locations were determined by making a thin wheel approximation and finding the intersection arc between the wheel and the local triangular mesh patches.

To study the omnidirectional capability of the robot, a desired 4.5 m square path was commanded at a constant speed of 1.5 m/s. This corresponds to 1.5 body lengths/second.

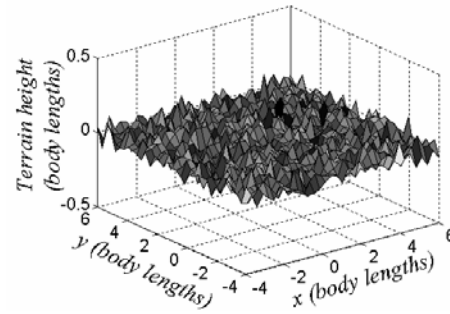


Figure 9. Example of terrain used in simulation, with  $\sigma = 4.5$ .

In the following simulations,  $\sigma$  was chosen as 0, 1.5, 3.0, and 4.5 cm, yielding maximum terrain inclination angles of approximately  $0^\circ$ ,  $20^\circ$ ,  $35^\circ$ , and  $45^\circ$ , respectively.

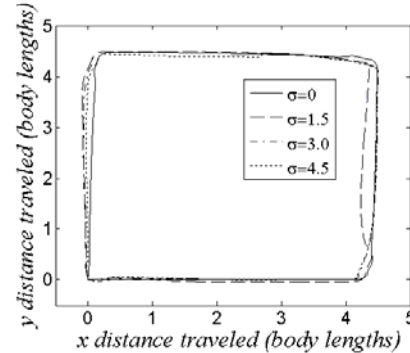


Figure 10. Top view of robot path during square tracking on rough terrain.

In Figure 10 it can be seen that the robot was able to track the desired path with relatively good fidelity, even in very rough terrain. Table III presents the RMS error for this trial for each terrain roughness.

TABLE III  
RMS PATH TRACKING ERROR FOR SEVERAL TERRAIN HEIGHTS

$\sigma$	0.0	1.5	3.0	4.5
RMS error (% body)	8.67	8.89	10.48	11.59

Further simulations were conducted to show the effects of

terrain knowledge in the controller and information of robot absolute position in the inertial frame. Simulations were run with and without absolute position updates at 0.5 Hz and with and without terrain knowledge. Simple dead reckoning was used estimate vehicle position when in simulations without absolute position information and to interpolate between updates for simulations with the information. Path tracking results are shown in Figure 11. Numerical results are shown in Table IV.

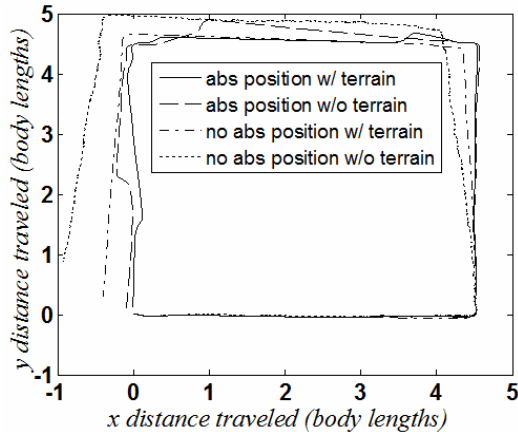


Figure 11. Top view of the body trace during square tracking on rough terrain for varying levels of controller knowledge.

TABLE IV  
RMS PATH TRACKING ERROR FOR VARYING CONTROLLER KNOWLEDGE

Controller	RMS error (% body)
Absolute position w/ terrain	6.96
Absolute position w/o terrain	17.71
No absolute position w/ terrain	21.28
No absolute position w/o terrain	86.31

When no absolute position information is available, a 75.3% reduction in path tracking error is seen when the vehicle controller uses terrain inclination information. The results indicate that in these simulations, utilizing terrain inclination information is nearly as good as having frequent absolute position updates. This is useful for the many situations where position information from GPS, for example, may be unavailable. Even with absolute position updates, path tracking error is reduced by 60.7% when the controller uses terrain information.

## VII. CONCLUSIONS

In this paper, the kinematics and control of an omnidirectional mobile robot driven by active split offset casters has been studied. Isotropy analysis indicates that a 2:1 split to offset length ratio yields a robot with equal mobility capability in all directions on flat terrain. On rough terrain, a larger ratio is desired, and robot isotropy degrades slightly. A kinematic controller was developed and its performance was studied on both flat and rough terrain. The effects of terrain information and inertial frame knowledge on performance were studied. Simulation results showed that the mobile robot was able to track a square trajectory with good performance despite local terrain inclinations

angles near 45°. It was also shown that path tracking improvements were possible if terrain information was used in the controller.

## REFERENCES

- [1] Fish, S., "UGV's in Future Combat Systems," *Proceedings of SPIE - The International Society for Optical Engineering*, v 5422, *Unmanned Ground Vehicle Technology VI*, pp. 288-291, Apr 2004.
- [2] Blitch, J., "Artificial Intelligence Technologies for Robot Assisted Urban Search and Rescue," *Expert Systems with Applications*, 1996.
- [3] Erickson, J., "Living the Dream: An Overview of the Mars Exploration Project," *IEEE Robotics and Automation Magazine*, v 13, n 2, pp. 12-18, Jun 2006.
- [4] Cheng, J., Gao, L., Wang, H., "Steering Analysis of Tracked Vehicles Based on Skid Condition," *Chinese Journal of Mechanical Engineering*, v 42, pp. 192-195, May 2006.
- [5] Lindemann, R., Bickler, D., Harrington, B., Ortiz, G., Voorhees, C., "Mars Exploration Rover Mobility Development - Mechanical Mobility Hardware Design, Development, and Testing," *IEEE Robotics and Automation Magazine*, v 13, n 2, pp. 19-26, Jun 2006.
- [6] Ishigami, G., Miwa, A., Yoshida, K., "Steering Trajectory Analysis of Planetary Exploration Rovers Based on All-Wheel Dynamics Model," *Proceedings of the 8th International Symposium on Artificial Intelligence, Robotics and Automation in Space*, pp. 121-128, 2005.
- [7] Iagnemma, K. and Dubowsky, S., *Mobile Robots in Rough Terrain: Estimation, Motion Planning, and Control with Application to Planetary Rovers*, Springer Tracts in Advanced Robotics (STAR) Series, Vol. 12, Springer, 2004.
- [8] Fujisawa, S., Ohkubo, K., Yoshida, T., Satonaka, N., Shidama, Y., and Yamaura, H., "Improved Moving Properties of an Omnidirectional Vehicle Using Stepping Motor", *Proceedings of the 36th Conference on Decision & Control*. San Diego, California, pp.3654-3657, 1997.
- [9] Williams, R., Carter, B., Gallina, P., and Rosati, G., "Wheeled Omnidirectional Robot Dynamics Including Slip," *Proceedings of 2002 ASME Design Engineering Technical Conferences*, Sep 2002.
- [10] Muir, P., and Neuman, C., "Kinematic Modeling for Feedback Control of an Omnidirectional Wheeled Mobile Robot," *Proc. of 1987 IEEE Int. Conf. on Robotics and Automation*, 1987
- [11] Bradley A., Miller, S., Creary, G., Miller, N., Begley, M., Misch, N., "Mobius, an Omnidirectional Robot Utilizing Mecanum Wheels and Fuzzy Logic Control," *Proceedings of the 28th Annual AAS Rocky Mountain Guidance and Control Conferences*, pp. 251-266, 2005.
- [12] Ferriere L., Rauceant B., "ROLLMOBS, a New Universal Wheel Concept," *Proceedings of 1998 IEEE International Conference on Robotics and Automation*, pp. 1877-1882, Leuven, May 1998.
- [13] West, A.M., and Asada, H., "Design of Ball Wheel Mechanisms for Omnidirectional Vehicles with Full Mobility and Invariant Kinematics," *ASME Journal of Mechanical Design*, 117, 1995.
- [14] Carlson, J., Murphy, R., "How UGVs Physically Fail in the Field," *IEEE Transactions on Robotics*, v 21, n 3, Jun 2005.
- [15] Wood, C., Davidson, M., Rich, S., Keller, J., and Maxfield, R., "T2 Omnidirectional Vehicle Mechanical Design," *Proc. of the SPIE Conference on Mobile Robots XIV*, Boston, pp. 69-76, Sep 1999.
- [16] Park, T., Lee, J., Yi, B., Kim, W., You, B., Oh., "Optimal Design and Actuator Sizing of Redundantly Actuated Omni-directional Mobile Robots," *IEEE International Conference on Robotics and Automation*, pp.732-737, 2002.
- [17] Yu, H., Dubowsky, S., and Skwersky, A., "Omni-directional Mobility Using Active Split Offset Castors." *Proceedings of the 26th Biennial Mechanisms and Robotics Conference of the 2000 ASME Design Engineering Technical Conferences*, Sep 2000.
- [18] Spenko, M., Yu, H., and Dubowsky, S., "Analysis and Design of an Omnidirectional Platform for Operation on Non-Ideal Floors," *Proceedings of the 2002 IEEE International Conference on Robotics and Automation (ICRA 02)*, Washington, DC, May 2002.
- [19] Iagnemma, K., Rzepniewski, A., Dubowsky, S., and Schenker, P., "Control of Robotic Vehicles with Actively Articulated Suspensions in Rough Terrain," *Autonomous Robots*, V 14, Num. 1, Jan 2003.